IEEE Access
Multidisciplinary | Rapid Review | Open Access Journal

Received February 21, 2020, accepted March 7, 2020, date of publication March 11, 2020, date of current version March 23, 2020.

Digital Object Identifier 10.1109/ACCESS.2020.2980010

Deception Approach to Track-to-Track Radar Fusion Using Noncoherent Dual-Source Jamming

BIN RAO[1,2], ZHAOYU GU[2], AND YUANPING NIE[3]

[1]School of Electronics and Communication Engineering, Sun Yat-sen University, Guangzhou 510006, China
[2]State Key Laboratory of Complex Electromagnetic Environment Effects on Electronics and Information System, National University of Defense Technology, Changsha 410073, China
[3]National Key Laboratory of Science and Technology on Information System, Beijing 100101, China

Corresponding author: Bin Rao (raozibin1026@sina.com)

This work was supported by the National Natural Science Foundation of China under Grant 61201335, Grant 61571451, and Grant 61701507.

ABSTRACT Dual-source jamming is an effective way to prevent monopulse radar systems from performing accurate angle measurements. In this investigation, based on noncoherent dual-source jamming, we propose a cooperative deception approach, which has the benefit of causing persistent and large angular measurement errors to protect a true target and therefore can greatly reduce the discrimination capability of a distributed track-to-track radar fusion system. A scenario involving a single target accompanied by a digital radio frequency memory (DRFM)-based repeater jammer countering two radar systems is illustrated. By controlling the amplitude ratio and time delay in a statistical manner, the active decoy signal and target echo signal can form a noncoherent angular glint effect and result in the deviation of the angle tracking loop of the two radar systems from the true target in opposite directions. The track-to-track association distance related to the retransmission parameters is explicitly derived, and its statistical characteristics are analyzed in detail. Simulations verify the feasibility of the approach. The advantage of the approach lies in its ability to destroy the so-called ''common origin'' signature of the physical target by injecting false angular information. The direct result is that the true target might not successfully complete the process of track-to-track association, thereby enabling us to realize the desirable effect of ''disguise the true target and instead show false decoys''.

INDEX TERMS Dual-source jamming, networked radar system, radar countermeasures, radar tracking, track-to-track fusion.

I. INTRODUCTION

In recent years, the technology of networked radar systems (also called multi-site radar systems, multiradar systems, multistatic radar systems, etc.) has received much attention and found wide use in many military and civilian applications [1]–[5]. These applications include air traffic control [6], military surveillance [7], meteorological monitoring [8], autonomous vehicles [9], and other complex systems. There is a growing awareness that ''fusion'' is of great value because of information redundancy and/or superposition.

The fundamental idea behind fusion is to make more effective use of the information contained in the spatial diversity of the electromagnetic field. The radar subsystems can be of different frequency bands, different programs (operating modes), different polarizations, and, most importantly, different locations. These integrated features of a networked radar system, such as the system mode, frequency, polarization, signal, and data fusion, all add up to a native ability to reject electronic countermeasures (ECMs) and/or clutter. Compared with simply improving the target location accuracy, the electronic counter-countermeasure (ECCM) ability of multiradar systems is of great importance for the survival and operation performance in electronic warfare. Networked radar systems using signal-fusion-based or data-fusion-based approaches to discriminate between physical targets and range deception jamming targets can be found in [10]–[14]. Some researchers even use the data fusion algorithm of a networked radar

The associate editor coordinating the review of this manuscript and approving it for publication was Heng Zhang.

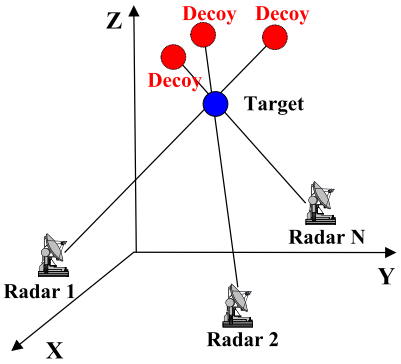

FIGURE 1. "Common origin" signature of a true target.

system to combat false data injection attacks when the intrusion detection is out of function [15].

In general, the multiradar fusion mode can be divided into several categories, such as centralized fusion [16]–[18], distributive (distributed) fusion [19]–[25], bistatic processing [26], [27], and passive location [28], [29]. Among these, the distributive radar fusion (or distributed tracking) is the most important and commonly used type of information fusion. For distributive fusion, each radar system employs an estimator to extract a target track and its associated covariance from its respective raw measurements, which are then transmitted by a data link to a fusion center. At the fusion center, the track-to-track association (or correlation) and track fusion are performed to obtain a composite target state estimation [2]. The track-to-track association is the workhorse of distributive fusion. In fact, compared with other types of fusion, the configuration of distributive fusion has a natural advantage in countering deception jamming. With the so-called "common origin" [19] signature of true targets (or, more precisely, physical targets because they actually exist in space), undesirable deception tracks and temporary tracks can be greatly reduced by using the key process of track-to-track association.

The underlying rationale lies in the fact that a physical target originates from a uniquely single point in space (i.e., borne from a "common origin"), irrespective of the radar positions and radar numbers, whereas it is difficult to make active decoys (mainly range deception decoys) also have this characteristic since they are physically nonexistent. This is illustrated in Fig. 1, where a true target observed from different radar systems will congregate around a single point in some space and be influenced only by radar measurement noises, whereas in general, active decoys do not have this unique characteristic. Therefore, a fusion center employing a simple track-to-track association can filter out most of these deception tracks, even if they can form stable tracks (actually, in some cases, it is difficult for decoys to form tracks due to imperfect retransmission). Essentially, it is the information redundancy that enables a distributed radar system to have a native active jamming resistance ability.

In contrast, from the viewpoint of ECMs, when countering networked radar systems, more challenges will occur, because it is difficult for a single jammer to jam all the multiradar subsystems due to the frequency diversity of the radar network. Even if the jamming bandwidth can cover the whole range of multiradar system frequencies and its power is sufficiently large, it is not easy for a single repeater jammer to form coincident false tracks (i.e., originating from a "common origin"). For the above reasons, it is very important to study ECM techniques against networked radar systems (in particular, distributed radar systems) in the jamming field, since this type of fusion has an inherent jamming resistance ability.

Generally, deception jamming can be divided into several types, such as range deception, velocity deception, and angle deception [30], [31]. These attack a specific radar function. Range or velocity deception of a repeater jammer can be realized simply by storing and regenerating the intercepted radar pulses using the emerging digital radio frequency memory (DRFM) technique [32], which can overload the radar processor with an excessive number of targets. Nonetheless, range or velocity deception has some inherent deficiencies. One of these drawbacks lies in the fact that the angle measurements of decoys are the same as those of the jammer itself when simply applying retransmission, i.e., both the jamming signals and the jammer skin echo come from the same angular direction; hence, the radar angle-tracking circuits are always locked onto the jammer, as shown in Fig. 1. For this reason, angle deception, if it can be realized in an effective way, seems to be more significant than range deception alone. However, for self-screening jamming (SSJ), angle deception jamming appears to be technically difficult due to the monopulse techniques commonly used in tracking radar systems [33]. Perhaps the most feasible angle deception method is dual-source jamming, which is based on the angular glint effect [30], [34], [35].

The dual-source jamming (interference) method is commonly used in radar countermeasures to counter anti-radiation missiles in airborne applications of towed decoys and in ground-based applications for radar self-protection. It is one of the most effective ways to defeat monopulse radar systems. Towed radar decoy and cross-eye jamming (CEJ) are two typical ways to carry out dual-source jamming. In essence, dual-source jamming involves forming a radar echo phase-front distortion and deceiving the radar angle measurements by making the radar receiving antenna receive two signals moving in different directions at the same time. To some extent, the traditional dual-source jamming method works well and can deceive single tracking radar effectively. However, this is not the case when attempting to deceive an entire networked radar system, as has been mentioned above. Therefore, if the dual-source jamming is used to jam individual radar devices independently without some cooperation, the fusion center might also use the "common origin" signature to discriminate these phantom tracks, irrespective of whether they are range or angle deceptions; therefore, the whole jamming effect will be greatly discounted.

To defeat networked radar systems, it is more appropriate to use the ''system versus system'' strategy, i.e., the attacking devices (including the jammers and targets) should also work cooperatively, and to form a ''jamming netting'' against a ''radar netting''. Thus, the cooperation and data link between a jammer and the target to be protected, as well as having some a priori information of threatening radar systems, are critical and necessary.

As far as the whole jamming effect is concerned, keeping the true target of interest from not being detected by each tracking radar system, and subsequently preventing it from being affirmed (judged as a threatened target) by the fusion center, is much more important than simply showing false target tracks in each radar scan without some cooperation.

For this reason (i.e., ''disguise true target''), this paper proposes a cooperative deception jamming approach to reduce the capability of distributive radar fusion and discrimination. To a large extent, it can result in the true target not passing the so-called ''common origin'' test and possibly being misjudged as a false target.

The principal contributions of this work are as follows:

(i) The statistical characteristics of noncoherent dual-source jamming as a function of different retransmitting amplitude ratios are analyzed.

(ii) The track-to-track association distance of true target tracks as a function of two retransmitted amplitude ratios is explicitly derived in an analytical way. It is found that the maximum association distance is directly proportional to the absolute value of the subtraction between the two linear deviations of the angular glint.

(iii) A guideline is provided as to what parameters should be used in specific scenarios according to theoretical analysis and simulations.

Nonetheless, to limit the scope of this research, we did make some reasonable assumptions to simplify the problem:

(i) The target detection probability is 1, and the false alarm probability is 0, i.e., we assume the target and decoys are ideally tracked by each radar system without misdetections and erroneous associations.

(ii) The jammer has a priori information of the radar positions as well as the target to be protected such that it can precisely control the delay and amplitude to form high-fidelity dual-source jamming.

Actually, assumption (i) considers a strong threat scenario, i.e., we ideally assume that each radar subsystem tracks and associates all the targets. Assumption (ii) can be easily realized by receiving the global positioning system (GPS) information of the target via a local communication link. In addition, the a priori information of radar positions can be obtained by means of reconnaissance. Although these additional requirements may more or less increase the complexity of the whole jamming system, it is worth doing this to realize the ''disguise true target'' purpose.

The remainder of this paper is organized as follows. Section II describes the statistical properties of dual-source jamming. Section III is the presented cooperative dual-source jamming method; a more detailed derivation of the analytical expression of the track-to-track association distance is also given. This is followed in Section IV by a simulation example. Concluding remarks are provided in the last section.

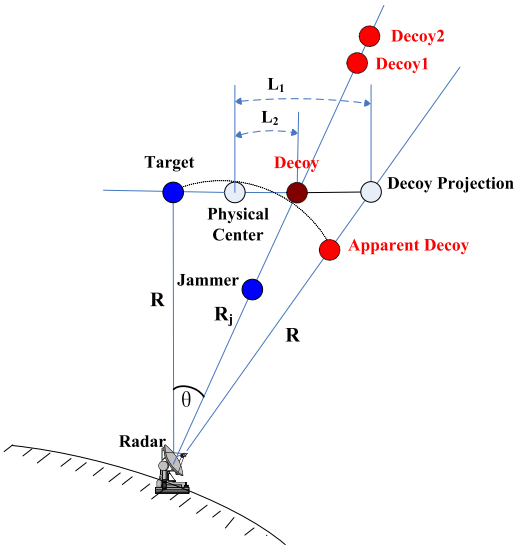

FIGURE 2. "Radar-Target-Decoy" geometry.

II. STATISTICAL PROPERTIES OF DUAL-SOURCE JAMMING

A. INTRODUCTION TO DUAL-SOURCE JAMMING

Dual-source jamming is one of the most commonly used methods to counter monopulse radar systems. The keystone of dual-source jamming is the angular glint: if the size of the target is close to the radar wavelength and it has two or more equivalent scattering centers, it will generate angular glint noises. The angular glint phenomenon is an inherent characteristic of radar extended targets and can give rise to large radar angular measurement errors. Since the concept of angular glint was put forward by D. D. Howard in 1950s, researchers have intensively investigated this well-known phenomenon. The linear deviation can represent this kind of glint noise [30].

Although the angular glint is initially used to account for the extended target's N-point scattering centers, it can also account for N-point source jamming, hence making it applicable for dual-source jamming.

For coherent or noncoherent dual-source jamming, we use Fig. 2 to illustrate the same idea. Due to the random variation in the relative amplitude and relative phase of the two sources, the phase-front of the electromagnetic wave will be distorted, and the linear deviation can indicate this distortion.

The linear deviation (or linear glint error) is defined as the ratio of the distance between the ''Physical Center'' and the ''Decoy'' to the distance between the ''Physical Center'' and the ''Decoy Projection''. ''Decoy Projection'' is defined as the crossover point between the line connecting the ''Radar'' to the ''Apparent Decoy'' (i.e., the target truly seen by the radar system) and the line connecting the ''Target'' to the ''Decoy''.

Note that in Fig. 2, the jammer is a repeater jammer that can generate multiple high-fidelity-range false targets (also called active decoys or decoys). In general, decoys can be generated at greater ranges than those of the jammer itself by delaying and then retransmitting a replica of the radar pulses. If the storage depth of the DRFM is adequate, one jammer can generate numerous decoys. However, decoys in a range smaller than that of the jammer itself require that the jammer be able to not only anticipate the appearance of the next radar pulse but also have knowledge of the pulse structure [36]. Therefore, in practical situations, the most commonly detected decoys are usually behind the jammer itself.

In Fig. 2, the solid blue points represent physical targets, which include the target (to be protected) and the jammer itself, and the dashed red points represent the decoys since they are non-real. Also note that in Fig. 2, for the sake of conciseness and brevity, we assume that the jammer generates only three decoys, i.e., "Decoy", "Decoy1", and "Decoy2", which are all generated by the same procedure of retransmission. For the false target "Decoy", it is generated by precisely controlling the time delay; therefore, the delay satisfies $\Delta R = R_j - R$, where R is the target range and R_j is the jammer range. Since the false "Decoy" and true "Target" have the same phase-front (their ranges are the same), the dual-source jamming effect naturally forms. However, other decoys (e.g., "Decoy1" and "Decoy2") cannot form dual-source jamming because there are no more than two sources contemporarily located in the same range bin as well as in the same beam angle.

According to the definition, the linear deviation e of Fig. 2 is obtained as

$$e = L_1/L_2 \tag{1}$$

Note that the linear deviation e is related to the amplitude ratio ρ and the relative phase φ of the two sources. The linear deviation has the following classic expression and has been derived in many references [35]:

$$e = \frac{1-\rho^2}{1+\rho^2+2\rho\cos(\varphi)} \tag{2}$$

where ρ is the amplitude ratio and φ is the relative phase.

From (2), we can analyze the relationship between e, ρ and φ. The curves of the linear deviation defined by (2) are shown in Fig. 3.

From Fig. 3 and equation (2), some conclusions are obvious:

(i) When $\varphi = 180°$, e can reach its maximum in theory, whereas when $\varphi = 0°$ or $\varphi = 360°$, e is at its minimum, and its value is irrespective of ρ.

(ii) When ρ is close to 1 and φ is approximately 180, the absolute value of e is very large, and its sign highly depends on $\rho \to 1^+$ or $\rho \to 1^-$.

(iii) When $\rho \to \infty$, we have $e \to -1$, no matter what the value of φ is; when $\rho \to 0$, we have $e \to 1$, also irrespective of φ. This result means that the radar observed

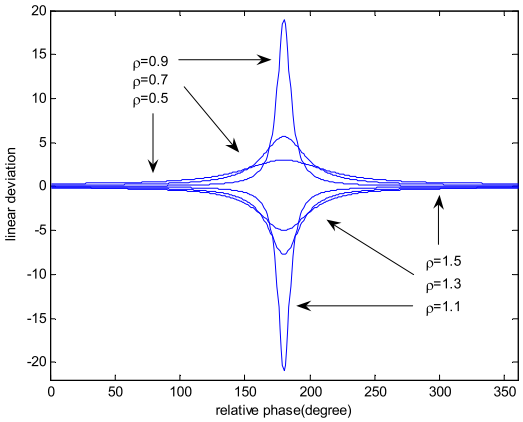

FIGURE 3. Linear deviation e with respect to ρ and φ.

line-of-sight (LOS) will sufficiently point to one source with a much larger amplitude.

From the preceding analysis, we can conclude that the ideal angle deception jamming process (for a single radar system) is to let the absolute value of the linear deviation (i.e., $|e|$) be as large as possible. However, for practical applications, the maximum of $|e|$ cannot exceed the radar beamwidth θ_w, since dual-source jamming is usually applicable for cases where the two sources are in the main beam. Any measurement values falling beyond the beamwidth will be treated as abnormal data and be discarded by sidelobe blanking. For escort jamming, such as ballistic penetration, the jammer and the target are usually deployed by a single payload, wherein the range between the jammer and the target is usually a few tens of kilometers, whereas the range from the jammer to the radar is hundreds of kilometers. Therefore, this scenario often satisfies the restriction since the penetration clouds are usually deliberately designed to confuse radar tracking in a single radar beam.

In addition, from (2), we can conclude that e can be controlled by both the amplitude ratio ρ and relative phase φ. Nonetheless, in reality, it is easy to control the amplitude ratio ρ, whereas it is difficult to control the relative phase φ. The reason partly lies in the fact that during the time from receiving to retransmission, the position and attitude of the airborne or missile-borne platform changes very quickly, wherein the path difference between the two signals will lead to a large disturbance. Furthermore, for practical engineering, because of sampling, digital processing, clock synchronization, and other reasons, the relative phase error of the two signals is also difficult to control. For these reasons, practical applications of dual-source jamming are generally noncoherent, especially for cases of independent sources (there is no towed cable). Thus, to a large extent, we consider only the out of phase case, i.e., the relative phase is assumed to be uniformly distributed in the interval $\varphi \in [0^o, 360^o]$. To sum up, if we want to have a desirable angular deception effect of two independent sources without some cable, the key is to control the relative ratio ρ of the dual source instead of its relative phase φ.

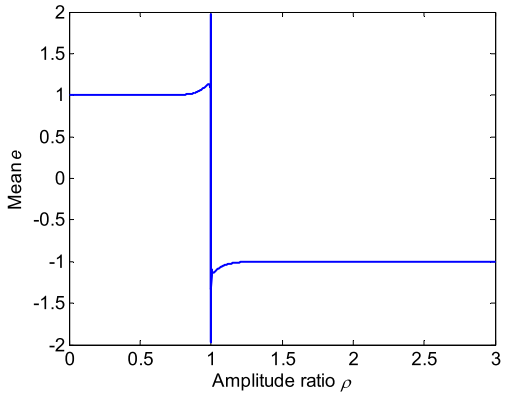

(a) Mean of e .

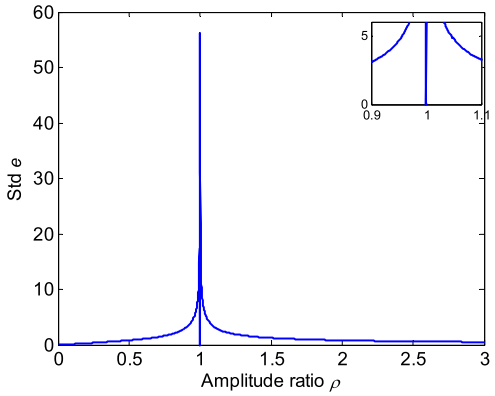

(b) std of e .

FIGURE 4. Statistical properties of the linear deviation. (a) Mean of *e*. (b) std of *e*.

B. STATISTICAL PROPERTIES OF THE LINEAR DEVIATION

Fig. 4 shows the statistical characteristics of the linear deviation e related to the amplitude ratio ρ from 10000 independent Monte Carlo simulations. The relative phase is assumed to be uniformly distributed in the interval $[0^o, 360^o]$. It can be seen that due to the randomness of the relative phase, e is indeed a random variable. Obviously, the ideal linear deviation should achieve a high mean while maintaining low variance (to guarantee the controllability). From Fig. 4(a), we know that when the amplitude ratio approaches 1, the mean of e can be any value from $-\infty$ to ∞. However, Fig. 4(b) illustrates that the standard deviation (std) is also very high, indicating that it is very difficult to control. It must be noted that when ρ is accurately equal to 1, the std is very low and approaches 0, which can be directly determined by (2). However, in reality, we cannot expect to control the amplitude ratio with this exactness because all types of errors extensively exist in real systems. Therefore, it is indeed still uncontrolled even if $\rho = 1$.

To sum up, from Fig. 4, when $\rho \in (0, 0.8)$, e is close to 1 and has a relatively lower std, whereas when $\rho \in (1.2, \infty)$, e is close to -1 and has a lower std. This phenomenon indicates that when $\rho \in (0, 0.8)$ or $\rho \in (1.2, \infty)$, we may expect to obtain some desirable angle deception effect with the smallest perturbations, i.e., sufficiently approaching one source or another.

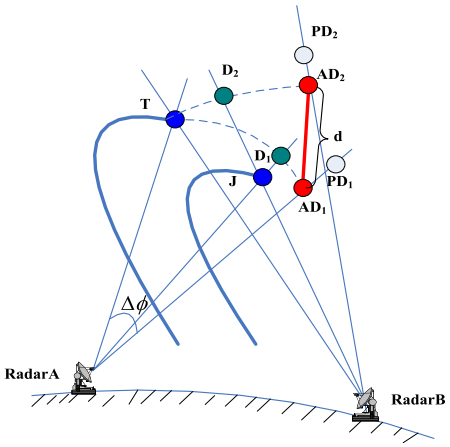

FIGURE 5. "Radar-target-jammer" geometry.

It must be noted that although in this investigation the attitude ratio ρ is considered as a deterministic quantity, in reality, it is not. In fact, because the true target radar cross-section (RCS) is a statistic quantity and is related to many factors, the amplitude ratio $\rho = \rho_{\text{Jammer}}/\rho_{\text{Target}}$ is essentially a random variable. Considering the fact that we have roughly known about the orders of the true target's RCS level, as long as the jammer power is more or less several times larger or smaller than that of the target signal, we can guarantee that the apparent false target will be close to the desired one of the dual sources.

III. COOPERATIVE DUAL-SOURCE ANGLE JAMMING METHOD

In this section, to reduce the fusion performance of the networked radar system, we analyze the track-to-track association distance of the true target between two radar systems. The association distance is directly determined by the two retransmitting amplitude ratios of the jammer, the interrelationship between which we will investigate here.

A. DERIVATION OF TRACK-TO-TRACK ASSOCIATION DISTANCE

For the sake of simplicity, we assume a scenario using a single target (e.g., airplane or reentry vehicle to be protected) accompanied by a single repeater jammer countering two radar systems. Furthermore, we assume that the two radar systems have common frequency bands, such that a single jammer can retransmit the echoes of the two radar systems simultaneously. Again, to avoid transformations between different radar-centered local coordinate systems (CSs), all the coordinates are described in the Earth-centered-fixed coordinate system (ECF-CS).

Fig. 5 shows that the distance from the apparent target (AD_1) to the radar system is equal to the distance between the true target (T) and the radar system, i.e., in the range dimension, there is no deception. Actually, only simultaneously

arriving signals coming from different directions (but also in the same beam) can form an accurate angular glint effect. Thus, to form an ideal angular glint effect, a navigation device (such as a GPS receiver) and a local communication device are necessary. If the jammer knows the coordinates of the radar systems, those of the true target, and its own position by using these devices, it can then accurately solve the delay parameters of the required decoys.

Assume that two radar sytems (radar A and radar B) are located at $\mathrm{R_A}(x_\mathrm{A}, y_\mathrm{A}, z_\mathrm{A})$ and $\mathrm{R_B}(x_\mathrm{B}, y_\mathrm{B}, z_\mathrm{B})$, respectively. Thus, we have

$$x_\mathrm{A}^2 + y_\mathrm{A}^2 + z_\mathrm{A}^2 = x_\mathrm{A}^2 + y_\mathrm{A}^2 + z_\mathrm{A}^2 = r_\mathrm{e}^2 \tag{3}$$

where r_e is the Earth average radius and a spherical Earth model is considered. Note that we have ignored the height of the radar systems because it is trivial when compared to the Earth radius.

Since in reality the positions of the target and the jammer are time-varying quantities due to movement, their positions are essentially related to time t. However, in the following derivation, to be more focused and concise, we ignore the time subscript "t". Denote the true position of the target as $\mathrm{T}(x, y, z)$ and that of the jammer as $\mathrm{J}(x_\mathrm{J}, y_\mathrm{J}, z_\mathrm{J})$. Note that both are physical targets. The decoy that is intended to form the dual-source jamming with the true target for radar A is denoted as $\mathrm{D}_1(x_1, y_1, z_1)$, and that for radar B is $\mathrm{D}_2(x_2, y_2, z_2)$. The decoy projection for radar A is denoted as $\mathrm{PD}_1(x_1^{\mathrm{PD}}, y_1^{\mathrm{PD}}, z_1^{\mathrm{PD}})$, and that for radar B is $\mathrm{PD}_2(x_2^{\mathrm{PD}}, y_2^{\mathrm{PD}}, z_2^{\mathrm{PD}})$. The apparent decoy for radar A is denoted as $\mathrm{AD}_1(x_1^{\mathrm{AD}}, y_1^{\mathrm{AD}}, z_1^{\mathrm{AD}})$, and that for radar B is $\mathrm{AD}_2(x_2^{\mathrm{AD}}, y_2^{\mathrm{AD}}, z_2^{\mathrm{AD}})$.

Because the true target (T) and decoy (D_1) can form dual-source jamming for radar A, we have

$$\begin{aligned}&(x - x_\mathrm{A})^2 + (y - y_\mathrm{A})^2 + (z - z_\mathrm{A})^2 \\ &\quad = (x_1 - x_\mathrm{A})^2 + (y_1 - y_\mathrm{A})^2 + (z_1 - z_\mathrm{A})^2 \triangleq R_1^2\end{aligned} \tag{4}$$

where R_1 denotes the range from the true target (T) to radar A. Thus, the delay range of the decoy (D_1) for radar A should satisfy

$$\begin{aligned}\Delta R_1 &\triangleq R_1 - R_{\mathrm{J}1} \\ &= \sqrt{(x - x_\mathrm{A})^2 + (y - y_\mathrm{A})^2 + (z - z_\mathrm{A})^2} \\ &\quad - \sqrt{(x_\mathrm{J} - x_\mathrm{A})^2 + (y_\mathrm{J} - y_\mathrm{A})^2 + (z_\mathrm{J} - z_\mathrm{A})^2}\end{aligned} \tag{5}$$

Similarly, the delay range of the decoy (D_2) for radar B should satisfy

$$\begin{aligned}\Delta R_2 &\triangleq R_2 - R_{\mathrm{J}2} \\ &= \sqrt{(x - x_\mathrm{B})^2 + (y - y_\mathrm{B})^2 + (z - z_\mathrm{B})^2} \\ &\quad - \sqrt{(x_\mathrm{J} - x_\mathrm{B})^2 + (y_\mathrm{J} - y_\mathrm{B})^2 + (z_\mathrm{J} - z_\mathrm{B})^2}\end{aligned} \tag{6}$$

Define the angular deviation $\Delta\phi$ as the LOS angle between the true target (T) and the apparent decoy (AD_1) direction. Thus, in a given range R, we know that $\Delta\phi$ is directly proportional to the linear deviation e.

The linear deviations of these two radar systems can be easily obtained. We denote them as e_1 (for radar A) and e_2 (for radar B); thus, we have

$$e_1 = \frac{1 - \rho_1^2}{1 + \rho_1^2 + 2\rho_1 \cos(\varphi_1)} \tag{7}$$

$$e_2 = \frac{1 - \rho_2^2}{1 + \rho_2^2 + 2\rho_2 \cos(\varphi_2)} \tag{8}$$

where ρ_1 and φ_1 are the amplitude ratio and relative phase, respectively, between the decoy and the true target for radar A. Similarly, ρ_2 and φ_2 are those quantities for radar B.

According to the basic geometrical relationship, we can obtain the coordinates of the decoy projection for radar A (i.e., PD_1) as

$$\begin{bmatrix} x_1^{\mathrm{PD}} \\ y_1^{\mathrm{PD}} \\ z_1^{\mathrm{PD}} \end{bmatrix} = \begin{bmatrix} 0.5(x + x_1) - 0.5e_1(x - x_1) \\ 0.5(y + y_1) - 0.5e_1(y - y_1) \\ 0.5(z + z_1) - 0.5e_1(z - z_1) \end{bmatrix} \tag{9}$$

Note that when $e_1 \to 1$, we have $\{x_1^{\mathrm{PD}} \to x_1, y_1^{\mathrm{PD}} \to y_1, z_1^{\mathrm{PD}} \to z_1\}$, which means that if the jammer power has absolute predominance, then the radar measurement angle is actually locked onto the jammer itself, whereas when $e_1 \to -1$, we have $\{x_1^{\mathrm{PD}} \to x, y_1^{\mathrm{PD}} \to y, z_1^{\mathrm{PD}} \to z\}$, which means that if the target amplitude has predominance, then the radar measurement angle is locked onto the true target itself. The analysis of e_2 also has this characteristic; for the sake of brevity, we do not list the equation here.

Note that the apparent decoy (AD_1) is also located in the same circle R_1, i.e.,

$$\begin{aligned}&(x_1^{\mathrm{AD}} - x_\mathrm{A})^2 + (y_1^{\mathrm{AD}} - y_\mathrm{A})^2 + (z_1^{\mathrm{AD}} - z_\mathrm{A})^2 \\ &\quad = (x - x_\mathrm{A})^2 + (y - y_\mathrm{A})^2 + (z - z_\mathrm{A})^2 \triangleq R_1^2\end{aligned} \tag{10}$$

Using the geometric proportional relationship, we can obtain the position of decoy (AD_1) as

$$\begin{aligned}\begin{bmatrix} x_1^{\mathrm{AD}} \\ y_1^{\mathrm{AD}} \\ z_1^{\mathrm{AD}} \end{bmatrix} &= \begin{bmatrix} x_\mathrm{A} + A_1(x_1^{\mathrm{PD}} - x_\mathrm{A}) \\ y_\mathrm{A} + A_1(y_1^{\mathrm{PD}} - y_\mathrm{A}) \\ z_\mathrm{A} + A_1(z_1^{\mathrm{PD}} - z_\mathrm{A}) \end{bmatrix} \\ &= \begin{bmatrix} x_\mathrm{A} + 0.5A_1\,[x + x_1 - e_1(x - x_1) - 2x_\mathrm{A}] \\ x_\mathrm{A} + 0.5A_1\,[y + y_1 - e_1(y - y_1) - 2y_\mathrm{A}] \\ z_\mathrm{A} + 0.5A_1\,[z + z_1 - e_1(z - z_1) - 2z_\mathrm{A}] \end{bmatrix}\end{aligned} \tag{11}$$

where A_1 is the ratio of the range from the decoy (AD_1) to radar A to the range from the decoy projection (PD_1) to radar A. A_1 is actually a time-varying quantity sufficiently approaching one and has the following expression:

$$A_1 \triangleq \frac{R_1}{R_1^{\mathrm{PD}}} = \frac{\sqrt{(x - x_\mathrm{A})^2 + (y - y_\mathrm{A})^2 + (z - z_\mathrm{A})^2}}{\sqrt{(x_1^{\mathrm{PD}} - x_\mathrm{A})^2 + (y_1^{\mathrm{PD}} - y_\mathrm{A})^2 + (z_1^{\mathrm{PD}} - z_\mathrm{A})^2}} \tag{12}$$

Similarly, we can obtain the coordinate of decoy projection (PD_2) for radar B as

$$\begin{bmatrix} x_2^{\mathrm{PD}} \\ y_2^{\mathrm{PD}} \\ z_2^{\mathrm{PD}} \end{bmatrix} = \begin{bmatrix} 0.5(x+x_2)-0.5e_2(x-x_2) \\ 0.5(y+y_2)-0.5e_2(y-y_2) \\ 0.5(z+z_2)-0.5e_2(z-z_2) \end{bmatrix} \tag{13}$$

and the position for decoy (AD_2) as

$$\begin{bmatrix} x_2^{\mathrm{AD}} \\ y_2^{\mathrm{AD}} \\ z_2^{\mathrm{AD}} \end{bmatrix} = \begin{bmatrix} x_{\mathrm{B}}+0.5A_2\,[x+x_2-e_2(x-x_2)-2x_{\mathrm{B}}] \\ y_{\mathrm{B}}+0.5A_2\,[y+y_2-e_2(y-y_2)-2y_{\mathrm{B}}] \\ z_{\mathrm{B}}+0.5A_2\,[z+z_2-e_2(z-z_2)-2z_{\mathrm{B}}] \end{bmatrix} \tag{14}$$

where

$$A_2 \triangleq \frac{R_2}{R_2^{\mathrm{PD}}} = \frac{\sqrt{(x-x_{\mathrm{B}})^2+(y-y_{\mathrm{B}})^2+(z-z_{\mathrm{B}})^2}}{\sqrt{(x_2^{\mathrm{PD}}-x_{\mathrm{B}})^2+(y_2^{\mathrm{PD}}-y_{\mathrm{B}})^2+(z_2^{\mathrm{PD}}-z_{\mathrm{B}})^2}} \tag{15}$$

Denote the track-to-track association distance between the apparent decoys (AD_1) and (AD_2) as d (the track-to-track association distance of the true target measured by two radar systems is apparent); thus, we have

$$d=\{[x_2^{\mathrm{AD}}-x_1^{\mathrm{AD}}]^2+[y_2^{\mathrm{AD}}-y_1^{\mathrm{AD}}]^2+[z_2^{\mathrm{AD}}-z_1^{\mathrm{AD}}]\}^{1/2} \tag{16}$$

Substitution of (11) and (14) into (16) and collection of the terms yield the following result:

$$\begin{aligned} d^2 = {} & 0.25\{A_2\,[x+x_2-e_2(x-x_2)-2x_{\mathrm{B}}] \\ & -A_1\,[x+x_1-e_1(x-x_1)-2x_{\mathrm{A}}]+2(x_{\mathrm{B}}-x_{\mathrm{A}})\}^2 \\ & +0.25\{A_2\,[y+y_2-e_2(y-y_2)-2y_{\mathrm{B}}] \\ & -A_1\,[y+y_1-e_1(y-y_1)-2y_{\mathrm{A}}]+2(y_{\mathrm{B}}-y_{\mathrm{A}})\}^2 \\ & +0.25\{A_2\,[z+z_2-e_2(z-z_2)-2z_{\mathrm{B}}] \\ & -A_1\,[z+z_1-e_1(z-z_1)-2z_{\mathrm{A}}]+2(z_{\mathrm{B}}-z_{\mathrm{A}})\}^2 \end{aligned} \tag{17}$$

(17) is considerably complicated. In fact, A_1 is implicitly related to e_1, and A_2 is implicitly related to e_2. Noting that, in reality, the distance from the target to the radar (several hundred kilometers) is much larger than that from the target to the jammer (usually several hundred meters), we can have the approximations $A_1 \approx 1$ and $A_2 \approx 1$. This is also demonstrated in Fig. 6 by a typical simulation where the maximum deviation is less than 0.0005 (these curves are obtained according to the simulation presented in Section IV). For the sake of brevity, the evolutionary curves of A_2 for radar B are not shown here since they have a similar characteristic.

Assuming $A_1 \approx 1$ and $A_2 \approx 1$, equation (17) reduces to

$$\begin{aligned} d^2 \approx {} & 0.25\,[e_1(x-x_1)-e_2(x-x_2)-(x_1-x_2)]^2 \\ & +0.25\,[e_1(y-y_1)-e_2(y-y_2)-(y_1-y_2)]^2 \\ & +0.25\,[e_1(z-z_1)-e_2(z-z_2)-(z_1-z_2)]^2 \end{aligned} \tag{18}$$

Obviously, to prevent the true target from being affirmed by the fusion center through the so-called "common origin" test, we should make $d = d(t)$ as large as possible. Actually, if the target is truly a physical target, the track-to-track distance $d(t)$ of different radar systems will be very small and perturbed only by the radar measurement noises, whereas if the targets are decoys, since they are ghost tracks generated by delay and retransmission, $d(t)$ might be very large and cannot pass the "common origin" test. Our purpose is to give the true target (to be protected) this "non-passing" characteristic.

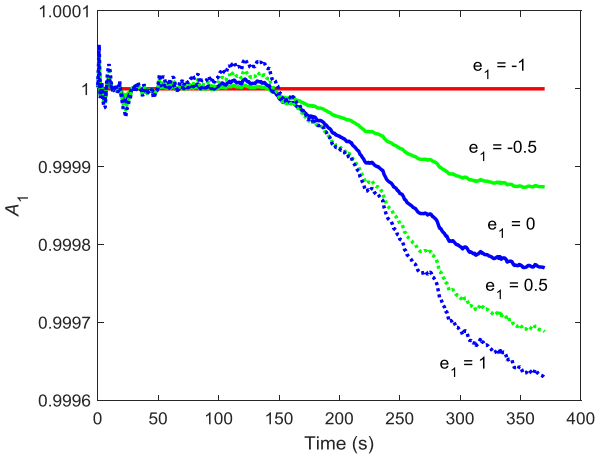

FIGURE 6. Parameter A_1 as a function of e_1.

B. CHARACTERISTICS OF $d(e_1, e_2)$

Next, the extreme value features of d are analyzed. The extreme value problem can be solved by using partial differentiation.

Taking the derivative of d^2 with respect to e_1, we obtain

$$\begin{aligned} & \frac{\partial d^2}{\partial e_1} \\ & = (x-x_1)[0.5e_1(x-x_1)-0.5e_2(x-x_2)+0.5(x_2-x_1)]^2 \\ & \quad +(y-y_1)[0.5e_1(y-y_1)-0.5e_2(y-y_2)+0.5(y_2-y_1)]^2 \\ & \quad +(z-z_1)[0.5e_1(z-z_1)-0.5e_2(z-z_2)+0.5(z_2-z_1)]^2 \end{aligned} \tag{19}$$

Similarly, for e_2, we have

$$\begin{aligned} & \frac{\partial d^2}{\partial e_2} \\ & = (x-x_2)[0.5e_1(x-x_1)-0.5e_2(x-x_2)+0.5(x_2-x_1)]^2 \\ & \quad +(y-y_2)[0.5e_1(y-y_1)-0.5e_2(y-y_2)+0.5(y_2-y_1)]^2 \\ & \quad +(z-z_2)[0.5e_1(z-z_1)-0.5e_2(z-z_2)+0.5(z_2-z_1)]^2 \end{aligned} \tag{20}$$

Define the target vector in the ECF-CS as $\mathbf{r} \triangleq (x, y, z)^{\mathrm{T}}$, decoy ($D_1$) for radar A as $\mathbf{r}_1 \triangleq (x_1, y_1, z_1)^{\mathrm{T}}$, and decoy ($D_2$) for radar B as $\mathbf{r}_2 \triangleq (x_2, y_2, z_2)^{\mathrm{T}}$. According to the derivatives of (19) and (20), we can draw some conclusions.

(i) For radar A, when $\mathbf{r} > \mathbf{r}_1$, we have $\partial d^2/\partial e_1 > 0$, i.e., d^2 monotonically increases with e_1, whereas when $\mathbf{r} < \mathbf{r}_1$, we have $\partial d^2/\partial e_1 < 0$, and d^2 monotonically decreases with e_1.

(ii) For radar B, when $\mathbf{r} > \mathbf{r}_2$, we have $\partial d^2/\partial e_2 > 0$, i.e., d^2 monotonically increases with e_2, whereas when $\mathbf{r} < \mathbf{r}_2$,

we have $\partial d^2/\partial e_2 < 0$, and d^2 monotonically decreases with e_2.

(iii) When $e_1 = -1$ and $e_2 = -1$, we have $\partial d^2/\partial e_1 = 0$ and $\partial d^2/\partial e_2 = 0$, irrespective of $\mathbf{r}, \mathbf{r}_1, \mathbf{r}_2$.

Taking the second derivative of d^2 with respect to e_1 and e_2, respectively, we have

$$\frac{\partial^2 d^2}{\partial e_1^2} = 0.5(x - x_1)^2 + 0.5(y - y_1)^2 + 0.5(z - z_1)^2 \geq 0 \tag{21}$$

$$\frac{\partial^2 d^2}{\partial e_2^2} = 0.5(x - x_2)^2 + 0.5(y - y_2)^2 + 0.5(z - z_2)^2 \geq 0 \tag{22}$$

Thus, the relationship between $d^2(e_1, e_2)$ and both e_1 and e_2 is actually a downward convex function. When $e_1 = -1$, $e_2 = -1$, it reaches the minimum value, i.e., $d^2 = 0$. In this case, the target power has predominance, whereas the jamming power can be neglected; hence, the radar beam is locked onto the true target itself.

For a downward convex function, its maximum appears at the boundaries. Because we know that $d^2(-1, -1) = 0$, the maximum should be one of the following:

$$d^2_{\max} = \max\{d^2(1, 1), d^2(-1, 1), d^2(1, -1)\} \tag{23}$$

According to (18), the three track-to-track association distances can be expanded as

$$d^2(1, 1) = (x_2 - x_1)^2 + (y_2 - y_1)^2 + (z_2 - z_1)^2 \tag{24}$$

$$d^2(1, -1) = (x - x_1)^2 + (y - y_1)^2 + (z - z_1)^2 \tag{25}$$

$$d^2(-1, 1) = (x - x_2)^2 + (y - y_2)^2 + (z - z_2)^2 \tag{26}$$

It is interesting that $d^2(1, 1)$ represents the distance between decoy (D_1) for radar A and decoy (D_2) for radar B, $d^2(1, -1)$ represents the distance between the true target (T) and decoy (D_1) for radar A, and $d^2(-1, 1)$ represents the distance between the true target (T) and decoy (D_2) for radar B. Thus, for noncoherent dual-source jamming, the optimum jamming effect is highly dependent on the target-jammer-radar geometry, which should be computed according to the specific scenario.

Next, a simple numerical experiment is carried out to verify the above analysis. We set $(e_1, e_2) \in [-1, 1] \times [-1, 1]$, $A_1 = 0.998$, and $A_2 = 0.997$, and the target and decoy positions $\mathbf{r}, \mathbf{r}_1, \mathbf{r}_2$ are randomly generated according to a typical scenario (see Section IV for details). Then, we obtain the numerical result, which is shown in Fig. 7.

From Fig. 7, it can be seen that d^2 is undoubtedly a downward convex function with a minimum $d^2(-1, -1) = 0$ over the interval $(e_1, e_2) \in [-1, 1] \times [-1, 1]$. The other three values are $d^2(-1, 1) = 4.8 \times 10^7 \text{km}^2$, $d^2(1, -1) = 4.9 \times 10^7 \text{km}^2$, and $d^2(1, 1) = 1.1 \times 10^5 \text{km}^2$. The result coincides with the above analytical derivations. Thus, equation (23) indeed indicates that to have an optimum jamming effect to counter distributive radar track fusion, we should try to deviate the angle tracking loops of the two radar systems from the true target in reversed directions. The best configuration is three points in a row wherein the true target is in the middle and the two decoys are at the ends. However, for political and military considerations, we cannot expect the radar-target-jammer geometry to form this unique and unusual configuration. Thus, in a more general case, the three points form an irregular triangle.

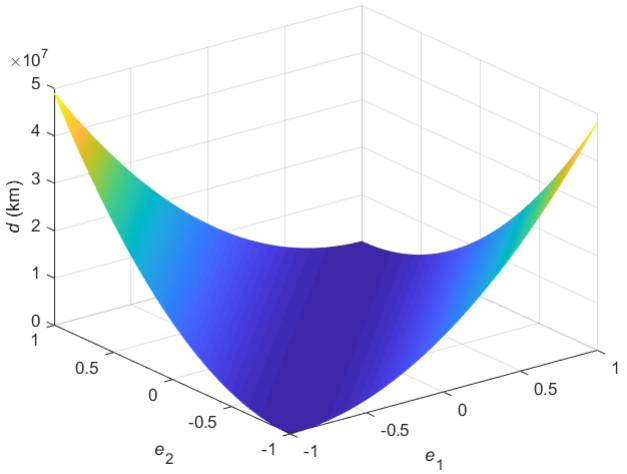

FIGURE 7. Effect of track-to-track distance d on e_1 and e_2.

C. CHARACTERISTICS OF $d(\rho_1, \rho_2)$

Note that our purpose is to maximize the track-to-track association distance $d(t)$ as much as possible such that the true target cannot be affirmed by the "common origin" test. To guide engineering applications, we should analyze the relationship of $d(\rho_1, \rho_2)$ instead of $d(e_1, e_2)$, since the relative phases φ_1 and φ_2 have not been considered.

In fact, from (18), we know that

$$d = d(e_1, e_2; \mathbf{r}, \mathbf{r}_1, \mathbf{r}_2) = d(\rho_1, \rho_2, \varphi_1, \varphi_2; \mathbf{r}, \mathbf{r}_1, \mathbf{r}_2) \tag{27}$$

At every time t, d is a stochastic process, mainly due to the randomness of the relative phases (actually, other quantities such as the positions are also random variables). Thus, to investigate the overall performance, we should analyze in a statistical way. The criterion is to evaluate the average track-to-track association distance d_{mean}, which is defined as the time average of two tracks via N Monte Carlo simulations. Let $d(i)$, $1 \leq i \leq N$ denote the discrete track-to-track association distance d related to two radar tracks using single-phase sampling values $\varphi_1(i)$, $\varphi_2(i)$, where $\varphi_1(i) \sim U[0^o, 360^o]$; $\varphi_2(i) \sim U[0^o, 360^o]$. Then, d_{mean} can be defined as

$$d_{\text{mean}} = \sum_{i=1}^{N} d(i)/N \tag{28}$$

Note that after averaging, d_{mean} indeed reduces to a function related to the two radar amplitudes, i.e.,

$$d_{\text{mean}} = d_{\text{mean}}(e_1, e_2; \mathbf{r}, \mathbf{r}_1, \mathbf{r}_2) = d_{\text{mean}}(\rho_1, \rho_2; \mathbf{r}, \mathbf{r}_1, \mathbf{r}_2) \tag{29}$$

where $\mathbf{r}, \mathbf{r}_1, \mathbf{r}_2$ are the known radar-target-decoy geometry at a given time, can be of any value but are deterministic due to a specific scenario.

Because the relative phases are not controllable, in the simulation, we assume that the relative phases are uniformly distributed in the interval of [0, 360]° and conduct massive Monte Carlo simulations to investigate the overall performance.

According to the scenario described above, we conduct a search among two possible amplitude ratios ρ_1 and ρ_2. The search interval is limited to $(\rho_1, \rho_2) \in [0, 2] \times [0, 2]$. The computation of $d(t)$ is done using (16); we repeat the Monte Carlo simulations 10000 times to obtain d_{mean} (the mean of the association distance) and d_{std} (the standard deviation of the association distance). The radar-target-decoy geometry parameters used are the following: $\mathbf{r} = (6451110, 0, 0)^{\text{T}}$, $\mathbf{r}_1 = (-506340.34, -224005.16, 56069.11)^{\text{T}}$, and $\mathbf{r}_2 = (-562158.53, 112847.49, 53783.07)^{\text{T}}$. In fact, these parameters are the initial parameters used in the scenario in Section IV.

A single run of the track-to-track association distance $d(\rho_1, \rho_2, \varphi_1, \varphi_2; \mathbf{r}, \mathbf{r}_1, \mathbf{r}_2)$ with respect to the above parameters $\mathbf{r}, \mathbf{r}_1, \mathbf{r}_2$ is shown in Fig. 8, where Fig. 8(a) is the 3D plot and Fig. 8(b) is the contour plot. Note that this picture shows only one random sampling of φ_1, φ_2.

It can be seen from Fig. 8 that, due to the randomness of the relative phase, the optimum track-to-track association distance d may not appear on the boundaries of the interval constraint of ρ_1 and ρ_2.Actually, in Fig. 8, the function $d(\rho_1, \rho_2)$ is multimodal (due to the influence of the phases) in the interval constraint $(\rho_1, \rho_2) \in [0, 2] \times [0, 2]$ with two local maximum values at roughly $(\rho_1, \rho_2) = (0.2, 1.9)$ and $(\rho_1, \rho_2) = (1.9, 0.2)$.

However, to instruct engineering practice, we cannot implement this exhaustive search as in Fig. 8 to find the optimal amplitude ratio combination. Alternatively, we use the statistical method to evaluate the probabilistic characteristics of d_{mean} on ρ_1 and ρ_2.

Fig. 9 shows the statistical mean and std of $d(\rho_1, \rho_2)$ after 10000 independent Monte Carlo runs of random phase generation, where Fig. 9(a) and Fig. 9(b) show the mean and std in 3D plots, respectively. From Fig. 9(a), we can observe that d_{mean} is much smaller in the intervals $(\rho_1, \rho_2) \in (0, 1) \times (0, 1)$ and $(\rho_1, \rho_2) \in (1, 2) \times (1, 2)$ when compared with the intervals $(\rho_1, \rho_2) \in (0, 1) \times (1, 2)$ and $(\rho_1, \rho_2) \in (1, 2) \times (0, 1)$. This observation indicates that in the former two intervals, the deception effect might not be satisfactory and thus might be discounted. The recommended intervals are the latter, i.e., $(\rho_1, \rho_2) \in (0, 1) \times (1, 2)$ and $(\rho_1, \rho_2) \in (1, 2) \times (0, 1)$, because d_{mean} is much larger. It also indicates an interesting fact: to disguise the true target such that it is not affirmed by a fusion center, we need to control only the two amplitude ratios such that one ratio is larger than one and the other is smaller than one, i.e., $\rho_1 > 1, \rho_2 < 1$ or $\rho_1 < 1, \rho_2 > 1$. This means that in a general noncoherent situation, the measured angle of one radar system should be

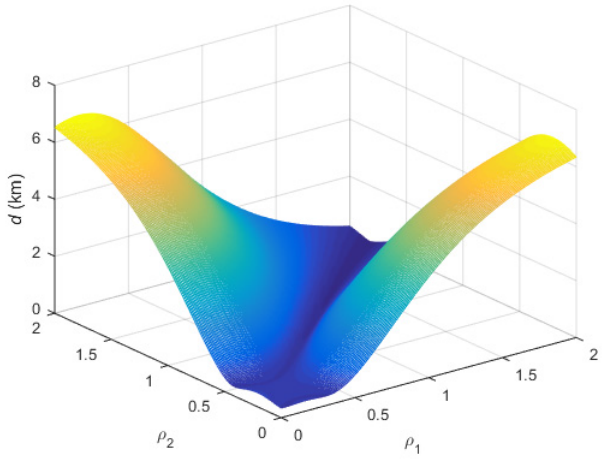

(a) 3D plot.

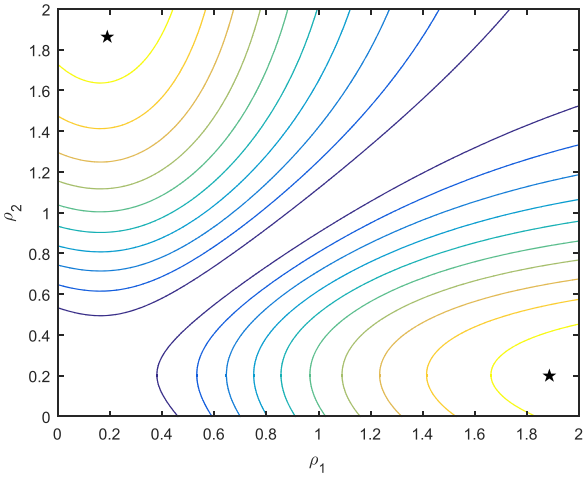

(b) Contour plot.

FIGURE 8. One random run of d on ρ_1 and ρ_2. (a) 3D plot. (b) Contour plot.

sufficiently close to the true target, while the other one should be close to a decoy for the other radar.

Next, we investigate the performance of d_{std}. Ideal cooperative jamming is to maximize d_{mean} while maintaining d_{std} at a lower level, which means better controllability to account for noncoherent influences of the phases. From Fig. 9(b), we know that we should try to avoid the point where $(\rho_1 = 1, \rho_2 = 1)$. Actually, in accordance with Fig. 4(b), we know that when ρ is at this point, although the linear deviation e can have a large mean, its std is also very high, i.e., its controllability is still much worse due to the influence of random phase noise.

To summarize, if the condition $\{\rho_1 > 1, \rho_2 < 1\}$ or $\{\rho_1 < 1, \rho_2 > 1\}$ is satisfied, then d_{mean} will be large and d_{std} will be relatively small in a statistical way. This guiding principle of selecting the parameters of the amplitude ratio can greatly decrease the fusion center discrimination ability for a true target. It must be pointed out that although the simulations are based on a specific radar-target-jamming

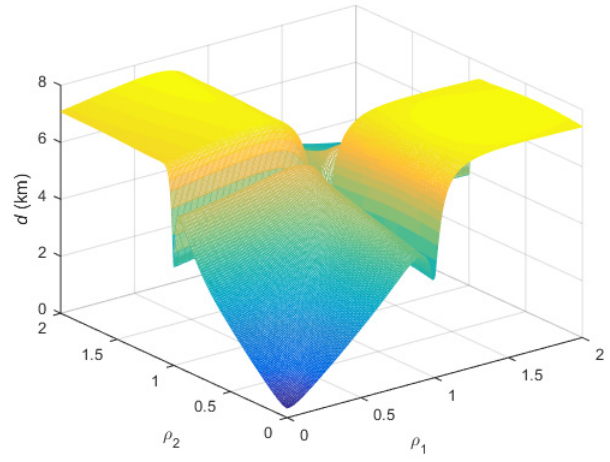

(a) Mean of $d(\rho_1, \rho_2)$ in the 3D plot.

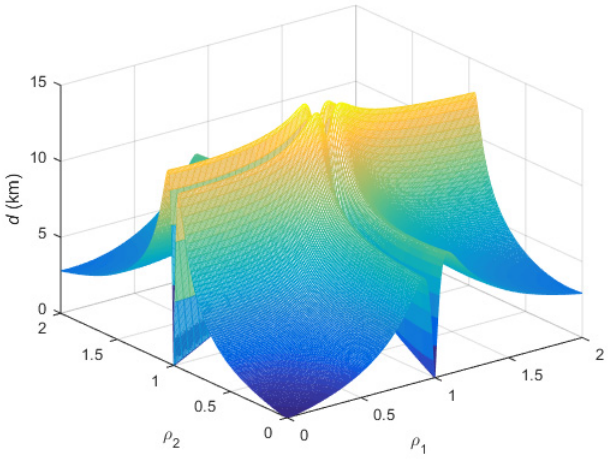

(b) std of $d(\rho_1, \rho_2)$ in the 3D plot.

FIGURE 9. Statistical relationship between d and both ρ_1 and ρ_2. (a) Mean of $d(\rho_1, \rho_2)$ in 3D plot; (b) std of $d(\rho_1, \rho_2)$ in 3D plot.

position ($\mathbf{r}$, $\mathbf{r}_1$, $\mathbf{r}_2$), the other formulations of the radar-target-jamming geometry also have similar results; we do not list these results for the sake of brevity. It can be seen from Fig. 4 that ($\rho_1 = 1$, $\rho_2 = 1$) is not a good choice because of larger variations in the mean and std.

It must be noted that although there is a lower mean and a larger std at the point ($\rho_1 = 1$, $\rho_2 = 1$), it does not mean that there is no deception effect. Actually, when ($\rho_1 = 1$, $\rho_2 = 1$), the deception point (apparent decoy) will have maximum randomness in the space, which may induce the target track to not be so smooth. In Fig. 9(a), even at ($\rho_1 = 1$, $\rho_2 = 1$), the track-to-track association distance d still has a value larger than 1.5 km; this will still have an influence on the fusion center discrimination and has a jamming effect.

IV. SIMULATIONS

In this section, we consider a comprehensive scenario of two radar systems tracking an exoatmospheric target to investigate the performance. Each radar system employs an extended Kalman filter (EKF) to track all the targets independently; then, the tracks of the two radars are collected and sent to the fusion center to implement the key process of track-to-track association. The presented cooperative jamming is then used to investigate the "common origin" performance of the true target.

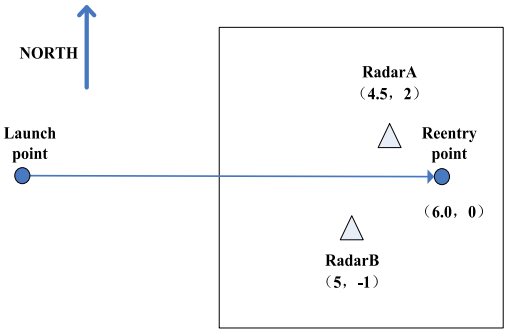

FIGURE 10. Simulation scenario.

A. SIMULATION SCENARIO DESCRIPTION

We assume a scenario involving a single target (a reentry vehicle) accompanied by a single repeater jammer countering two radar systems. The target and the jammer have similar trajectories, both follow the Keppler two-body curves, and no thrust and drag are experienced [37]. The initial reference velocity, altitude, and optimal tilt angle are 2500 m/s, 80 km, and 40.3070°, respectively. A spherical Earth model is considered. The jammer is assumed to be a self-screening repeater jammer close to the target. The initial distance between the target and the jammer is assumed to be 1000 m, and the other parameters are the same as those discussed earlier. The initial thrust cut-off points are both at 0°N latitude 0°E longitude, and the reentry points are at approximately 0°N latitude 6°E longitude. The total flying time is approximately 370 s of exoatmospheric flight, and the flying range is approximately 670 km.

We assume that the two radar systems are ground-based and with common frequency bands such that a single jammer can jam both radar systems. The radar positions are known a priori (radar A is positioned at 2.0°N latitude 4.5°E longitude, and radar B is positioned at −1°N latitude 5.0°E longitude), and their surveillance ranges are larger than 1000 km; hence, the two radar systems can cover the whole exoatmospheric phase. The range measurement accuracy is $\sigma_R = 10$m, the angle accuracy is $\sigma_A = \sigma_E = 1$mard, and the tracking data rate is 1 Hz for both radar systems. Due to the dynamics and measurement nonlinearities, the two radar systems employ the EKF [38]–[43] to form individual tracks. Furthermore, to simplify the problem, the detection probability is assumed to be 1, and the false alarm probability is 0. The nearest neighbor (NN) track-to-track association [3] method is employed in the fusion center to implement the track-to-track association.

The radar-target geometry is shown in Fig. 10. Note that the two radar systems do not necessarily need to be located

on reverse sides of the launching plane; other general deployments are also possible.

B. INDIVIDUAL EKF TRACKING STEPS

During the exoatmospheric phase, the predominant force acting on the target is Earth's gravity, while the effect of atmospheric drag and the gravitational forces due to other celestial bodies can be ignored. For tracking purposes, it is often preferable and necessary to formulate the motion of the target in the natural radar East-North-Up coordinate system (ENU-CS) [37]. Let $\mathbf{r}^{\mathrm{ENU}} \triangleq (x_{\mathrm{ENU}}, y_{\mathrm{ENU}}, z_{\mathrm{ENU}})^{\mathrm{T}}$, $\mathbf{v}^{\mathrm{ENU}} \triangleq \dot{\mathbf{r}}^{\mathrm{ENU}} \triangleq (\dot{x}_{\mathrm{ENU}}, \dot{y}_{\mathrm{ENU}}, \dot{z}_{\mathrm{ENU}})^{\mathrm{T}}$, and $\mathbf{a}^{\mathrm{ENU}} \triangleq \dot{\mathbf{v}}^{\mathrm{ENU}} = \ddot{\mathbf{r}}^{\mathrm{ENU}} = (\ddot{x}_{\mathrm{ENU}}, \ddot{y}_{\mathrm{ENU}}, \ddot{z}_{\mathrm{ENU}})^{\mathrm{T}}$ denote the target position, velocity, and acceleration in the ENU-CS, respectively; then, the acceleration model of the targets can be described by the following compact equation [37]:

$$\mathbf{a}^{\mathrm{ENU}} = -(\frac{\mu}{R_e^3}\mathbf{I}_{3\times 3} + \omega^2 \mathbf{\Phi}_2)(\mathbf{r}^{\mathrm{ENU}} + \boldsymbol{\xi}) - 2\omega \mathbf{\Phi}_1 \dot{\mathbf{r}}^{\mathrm{ENU}} \tag{30}$$

with

$$\mathbf{\Phi}_1 = \begin{bmatrix} 0 & -\sin B & \cos B \\ \sin B & 0 & 0 \\ -\cos B & 0 & 0 \end{bmatrix} \tag{31}$$

$$\mathbf{\Phi}_2 = \begin{bmatrix} -1 & 0 & 0 \\ 0 & -\sin^2 B & \sin B \cos B \\ 0 & \sin B \cos B & -\cos^2 B \end{bmatrix} \tag{32}$$

$$R_{\mathrm{e}} = [x_{\mathrm{ENU}}^2 + y_{\mathrm{ENU}}^2 + (z_{\mathrm{ENU}} + r_{\mathrm{e}} + H)^2]^{1/2} \tag{33}$$

where $\mathbf{I}_{3\times 3}$ denotes the 3×3 identity matrix, $\mu = 3.986005 \times 10^{14}\mathrm{m}^3/\mathrm{s}^2$ is the Earth's gravitational constant, $r_{\mathrm{e}} = 6378110\,\mathrm{m}$ is the average radius of the Earth, $\omega = 7.292115\mathrm{rad/s}$ is the Earth's rotational rate, $\boldsymbol{\xi} = (0, 0, r_{\mathrm{e}} + H)^{\mathrm{T}}$, and L, B, and H are the known radar longitude, latitude, and altitude, respectively. This model is adequate, as it considers the effect of the Earth's rotation.

In practice, measurements (observations) are usually available at discrete time instants. Let $\mathbf{Z}_k \triangleq (R_k, A_k, E_k)^{\mathrm{T}}$ be the measurement vector at time instant k (i.e., t_k); then, the measurement model is given by

$$\mathbf{Z}_k = \begin{bmatrix} R_k \\ A_k \\ E_k \end{bmatrix} = \begin{bmatrix} \sqrt{x_{\mathrm{ENU},k}^2 + y_{\mathrm{ENU},k}^2 + z_{\mathrm{ENU},k}^2} + w_R(k) \\ \tan^{-1}\dfrac{y_{\mathrm{ENU},k}}{x_{\mathrm{ENU},k}} + w_A(k) \\ \tan^{-1}\dfrac{z_{\mathrm{ENU},k}}{\sqrt{x_{\mathrm{ENU},k}^2 + y_{\mathrm{ENU},k}^2}} + w_E(k) \end{bmatrix} \tag{34}$$

where $w_R(k)$, $w_A(k)$, and $w_E(k)$ are the measurement noises of the radar at time instant k. For convenience, these noises are modeled as zero-mean and white Gaussian random processes with known error standard deviations $\sigma_R(k)$, $\sigma_A(k)$, and $\sigma_E(k)$, respectively. The measurement noises at different times as well as those of distinct observations are all assumed to be mutually independent.

It is well known that the ballistic target tracking is a problem of stochastic nonlinear filtering due to both the dynamics and measurement nonlinearities. As is reported in [41], from the tracking accuracy point of view, the nonlinear filters, e.g., EKF, unscented Kalman filter (UKF), and particle filter (PF), all appear to be statistically efficient (converge to a zero bias with an error standard deviation close to the Cramer-Rao lower bound (CRLB)). Among all these filters, the EKF is the preferred filter, as it combines statistical efficiency with the lowest computational load [41]. Therefore, in this context, we select the EKF to execute the tracking algorithms. For more detailed information on the EKF for ballistic target tracking, especially for the expanded forms of the Jacobians, the readers are referred to [38]–[44].

C. COORDINATE REGISTRATION

Note that the EKF steps are implemented in each radar local ENU-CS. To execute the so-called "common origin" test, these tracks must be converted to a common CS, which is generally the local fusion center ENU-CS or the global ECF-CS. In addition, before fusion, the time instants of each radar system should be registered with a common time reference. In this research, we simply assume that the time synchronization has been accomplished by using interpolation or other approaches.

The covariance $\mathbf{P}_{k|k}^{\mathrm{ENU}}$ of the estimated state vector $\hat{\mathbf{X}}_{k|k}^{\mathrm{ENU}} = [(\hat{\mathbf{r}}_{k|k}^{\mathrm{ENU}})^{\mathrm{T}}, (\hat{\mathbf{r}}_{k|k}^{\mathrm{ENU}})^{\mathrm{T}}]^{\mathrm{T}}$ (in the ENU-CS) at time instant k can be decomposed into blocks according to the position and velocity:

$$\mathbf{P}_{k|k}^{\mathrm{ENU}} = \begin{bmatrix} [\mathbf{P}_{k|k}^{\mathrm{ENU}}]_{\mathbf{rr}} & [\mathbf{P}_{k|k}^{\mathrm{ENU}}]_{\mathbf{rv}} \\ [\mathbf{P}_{k|k}^{\mathrm{ENU}}]_{\mathbf{vr}} & [\mathbf{P}_{k|k}^{\mathrm{ENU}}]_{\mathbf{vv}} \end{bmatrix} \tag{35}$$

where $[\mathbf{P}_{k|k}^{\mathrm{ENU}}]_{\mathbf{rv}} = [\mathbf{P}_{k|k}^{\mathrm{ENU}}]_{\mathbf{vr}}$ denotes the 3×3 cross-covariance of the position and velocity and $[\mathbf{P}_{k|k}^{\mathrm{ENU}}]_{\mathbf{rr}}$ and $[\mathbf{P}_{k|k}^{\mathrm{ENU}}]_{\mathbf{vv}}$ are the covariance of the position and velocity, respectively. When transformed to the ECF-CS, the total coordinate transformations of the state vector and covariance are obtained as

$$\begin{aligned} \hat{\mathbf{X}}_{k|k} &\triangleq \hat{\mathbf{X}}_{k|k}^{\mathrm{ECF}} \\ &= \{[\mathbf{T}_{\mathrm{ENU}}^{\mathrm{ECF}}(\hat{\mathbf{r}}_{k|k}^{\mathrm{ENU}} + \boldsymbol{\zeta})]^{\mathrm{T}}, (\mathbf{T}\hat{\mathbf{r}}_{k|k}^{\mathrm{ENU}})^{\mathrm{T}}\}^{\mathrm{T}} \end{aligned} \tag{36}$$

$$\begin{aligned} \mathbf{P}_{k|k} &\triangleq \mathbf{P}_{k|k}^{\mathrm{ECF}} \\ &= \begin{bmatrix} \mathbf{T}_{\mathrm{ENU}}^{\mathrm{ECF}}[\mathbf{P}_{k|k}^{\mathrm{ENU}}]_{\mathbf{rr}}[\mathbf{T}_{\mathrm{ENU}}^{\mathrm{ECF}}]^{\mathrm{T}} & \mathbf{T}_{\mathrm{ENU}}^{\mathrm{ECF}}[\mathbf{P}_{k|k}^{\mathrm{ENU}}]_{\mathbf{rv}}[\mathbf{T}_{\mathrm{ENU}}^{\mathrm{ECF}}]^{\mathrm{T}} \\ \mathbf{T}_{\mathrm{ENU}}^{\mathrm{ECF}}[\mathbf{P}_{k|k}^{\mathrm{ENU}}]_{\mathbf{vr}}[\mathbf{T}_{\mathrm{ENU}}^{\mathrm{ECF}}]^{\mathrm{T}} & \mathbf{T}_{\mathrm{ENU}}^{\mathrm{ECF}}[\mathbf{P}_{k|k}^{\mathrm{ENU}}]_{\mathbf{vv}}[\mathbf{T}_{\mathrm{ENU}}^{\mathrm{ECF}}]^{\mathrm{T}} \end{bmatrix} \end{aligned} \tag{37}$$

where $\mathbf{T}_{\mathrm{ENU}}^{\mathrm{ECF}}$ is an orthogonal transformation matrix, defined as

$$\mathbf{T}_{\mathrm{ENU}}^{\mathrm{ECF}} = \begin{bmatrix} -\sin(L) & -\sin(B)\cos(L) & \cos(B)\cos(L) \\ \cos(L) & -\sin(B)\sin(L) & \cos(B)\sin(L) \\ 0 & \cos(B) & \sin(B) \end{bmatrix} \tag{38}$$

$\boldsymbol{\zeta}$ is the local radar position described in the ECF-CS, i.e.,

$$\boldsymbol{\zeta} = \begin{bmatrix} (r_{\mathrm{e}} + H)\cos(B)\cos(L) \\ (r_{\mathrm{e}} + H)\cos(B)\sin(L) \\ (r_{\mathrm{e}} + H)\sin(B) \end{bmatrix} \tag{39}$$

D. TRACK-TO-TRACK ASSOCIATION

This subsection describes the implementation of the track-to-track association, which is the workhorse of the "common origin" test. The purpose is to test whether any two tracks pertain to the same (physical) target or not. For details, the readers are referred to [3].

Denote $\hat{\mathbf{X}}^{\mathrm{A}}_{k|k} = [(\hat{\mathbf{r}}^{\mathrm{A}}_{k|k})^{\mathrm{T}}, (\hat{\dot{\mathbf{r}}}^{\mathrm{A}}_{k|k})^{\mathrm{T}}]^{\mathrm{T}}$ and $\hat{\mathbf{X}}^{\mathrm{B}}_{k|k} = [(\hat{\mathbf{r}}^{\mathrm{B}}_{k|k})^{\mathrm{T}}, (\hat{\dot{\mathbf{r}}}^{\mathrm{B}}_{k|k})^{\mathrm{T}}]^{\mathrm{T}}$ as the converted estimated states of radar A and radar B in the ECF-CS, respectively. The corresponding converted covariances are denoted as $\mathbf{P}^{\mathrm{A}}_{k|k}$ and $\mathbf{P}^{\mathrm{B}}_{k|k}$.

Then, the state estimation errors are

$$\tilde{\mathbf{X}}^{\mathrm{A}}_{k|k} = \mathbf{X}^{\mathrm{A}}_{k|k} - \hat{\mathbf{X}}^{\mathrm{A}}_{k|k} \tag{40}$$

$$\tilde{\mathbf{X}}^{\mathrm{B}}_{k|k} = \mathbf{X}^{\mathrm{B}}_{k|k} - \hat{\mathbf{X}}^{\mathrm{B}}_{k|k} \tag{41}$$

Note that when the observed noises are not considered, the true value of the target should satisfy $\mathbf{X}_k \triangleq \mathbf{X}_{k|k} = \mathbf{X}^{\mathrm{A}}_{k|k} = \mathbf{X}^{\mathrm{B}}_{k|k}$, i.e., it is irrespective of the radar positions in the ECF-CS.

Denote the difference in the two estimations as

$$\hat{\mathbf{\Delta}}^{\mathrm{AB}}_{k|k} = \hat{\mathbf{X}}^{\mathrm{A}}_{k|k} - \hat{\mathbf{X}}^{\mathrm{B}}_{k|k} \tag{42}$$

This is the estimation of the difference between the true states

$$\mathbf{\Delta}^{\mathrm{AB}}_{k|k} = \mathbf{X}^{\mathrm{A}}_{k|k} - \mathbf{X}^{\mathrm{B}}_{k|k} = \mathbf{0}_{6\times 6} \tag{43}$$

The hypothesis of the "common origin test" is that

$$\begin{cases} H_0 : \mathbf{\Delta}^{\mathrm{AB}}_{k|k} = \mathbf{0}_{6\times 6}, \text{common origin} \\ H_1 : \mathbf{\Delta}^{\mathrm{AB}}_{k|k} \neq \mathbf{0}_{6\times 6}, \text{not common origin} \end{cases} \tag{44}$$

Denote the error in the difference between state estimates as

$$\tilde{\mathbf{\Delta}}^{\mathrm{AB}}_{k|k} = \mathbf{\Delta}^{\mathrm{AB}}_{k|k} - \hat{\mathbf{\Delta}}^{\mathrm{AB}}_{k|k} \tag{45}$$

Then, $\tilde{\mathbf{\Delta}}^{\mathrm{AB}}_{k|k}$ is the zero mean with covariance

$$\mathbf{T}^{\mathrm{AB}}_{k|k} \triangleq \mathrm{E}\{\tilde{\mathbf{\Delta}}^{\mathrm{AB}}_{k|k}[\tilde{\mathbf{\Delta}}^{\mathrm{AB}}_{k|k}]^{\mathrm{T}}\} = \mathrm{E}\{[\tilde{\mathbf{X}}^{\mathrm{A}}_{k|k} - \tilde{\mathbf{X}}^{\mathrm{B}}_{k|k}][\tilde{\mathbf{X}}^{\mathrm{A}}_{k|k} - \tilde{\mathbf{X}}^{\mathrm{B}}_{k|k}]^{\mathrm{T}}\} \tag{46}$$

Because the two radar systems independently measure the target, under the error independence assumption, we have

$$\mathbf{T}^{\mathrm{AB}}_{k|k} = \mathbf{P}^{\mathrm{A}}_{k|k} + \mathbf{P}^{\mathrm{B}}_{k|k} \tag{47}$$

Assume that the EKF is statistically efficient and that the estimation errors are still approximately Gaussian; then, the test statistic is

$$\hat{D}_{k|k} \triangleq [\hat{\mathbf{\Delta}}^{\mathrm{AB}}_{k|k}]^{\mathrm{T}}[\mathbf{T}^{\mathrm{AB}}_{k|k}]^{-1}\hat{\mathbf{\Delta}}^{\mathrm{AB}}_{k|k} \tag{48}$$

Then, the judgment is obtained as

$$\begin{cases} \hat{D}_{k|k} \leq D_\alpha, & \text{reject } H_0 \\ \hat{D}_{k|k} > D_\alpha, & \text{accept } H_1 \end{cases} \tag{49}$$

where the threshold D_α satisfies $P\left\{\hat{D}_{k|k} > D_\alpha | H_0\right\} = \alpha$ and, in the case of the Gaussian assumption, we have

$$D_\alpha = \chi^2_6(1-\alpha) \tag{50}$$

Note that the above derivations are the steps of the optimal track-to-track association test. The computational and memory requirements are relatively large. A simplified version would be to use only the position component to implement the test. The track-to-track association distance at time t_k related to the estimations of the two radar systems in the ECF-CS is as follows:

$$\begin{aligned} \hat{d}^1_k &= |\hat{\mathbf{r}}^{\mathrm{A}}_{k|k} - \hat{\mathbf{r}}^{\mathrm{B}}_{k|k}| \\ &= \{[\hat{x}^{\mathrm{A}}_{k|k} - \hat{x}^{\mathrm{B}}_{k|k}]^2 + [\hat{y}^{\mathrm{A}}_{k|k} - \hat{y}^{\mathrm{B}}_{k|k}]^2 + [\hat{z}^{\mathrm{A}}_{k|k} - \hat{z}^{\mathrm{B}}_{k|k}]\}^{1/2} \end{aligned} \tag{51}$$

The weighted track-to-track association distance is

$$\hat{d}^2_k = (\hat{\mathbf{r}}^{\mathrm{A}}_{k|k} - \hat{\mathbf{r}}^{\mathrm{B}}_{k|k})^{\mathrm{T}}[\mathbf{P}^{\mathrm{A}}_{k|k} + \mathbf{P}^{\mathrm{B}}_{k|k}]^{-1}_{\mathbf{rr}}(\hat{\mathbf{r}}^{\mathrm{A}}_{k|k} - \hat{\mathbf{r}}^{\mathrm{B}}_{k|k}) \tag{52}$$

Note that $\hat{d}^2_k$ is actually chi-square distributed with a freedom of 3 and that the test threshold is $d_\alpha = \chi^2_3(1-\alpha)$.

Among all the three testing statistics, $\hat{D}_{k|k}$ is the optimal one, $\hat{d}^1_k$ is the most intuitive and simplest, and $\hat{d}^2_k$ is modest. Actually, when the performance is considered, there is no significant difference between these three statistical tests, as all three tests consider the most important issue: position association.

A more practical operation of the fusion center is as follows: First, associate all tracks of radar A with those of radar B, and record the results of the hypothesis test and the track-to-track association distances of all comparisons. Second, make a unified judgment according to the same standard. If there are multiple tracks of radar B associated with a single track of radar A, then choose the smallest one (based on the track-to-track association distance) of radar B as the matched track. After these two steps, each track of radar A is either associated with a radar B track or not associated with any tracks of radar B. Tracks that can pass the hypothesis test (i.e., "common origin" test) can be considered as the most likely to originate from the physical targets, while tracks that do not associate with any tracks are considered as originating from jamming or clutter.

E. TRACKING AND FUSION RESULTS

From the above analysis, we know that, apart from precisely controlling the retransmitted time delay, controlling the amplitude of jamming such that it is several times larger or smaller than the target return is also crucial. Thus, by controlling the amplitude ratio and time delay, one might have the desirable deception effects in the fusion center, i.e., the retransmitted signal and target echo signal can form the angular glint effect, which might cause a deviation of the angle tracking loop of both radar systems from the true target in opposite directions.

Next, we analyze the tracking and fusion performance of the fusion center. We assume that the jammer can counter both radar systems. For the sake of conciseness and brevity, only one other decoy track (range false target) is considered in the simulation. Thus, each radar system can obtain three tracks, wherein two are physical targets (true target and the jammer itself) and one is the range false target (generated

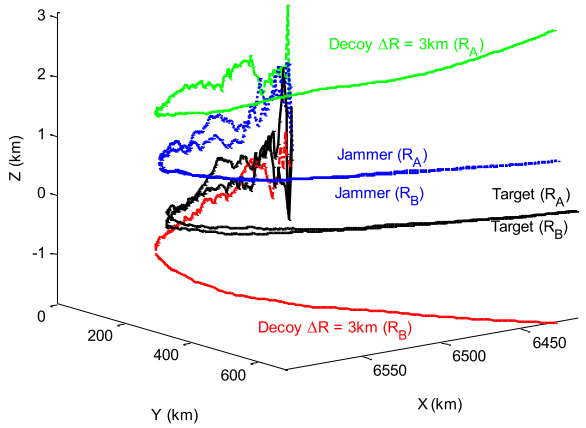

(a) Traditional method.

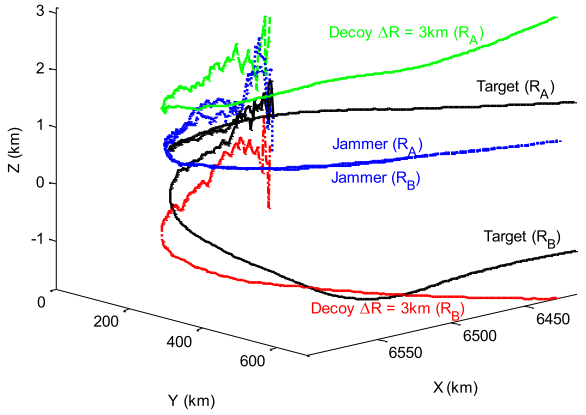

(b) New method.

FIGURE 11. All tracks in the fusion center (ECF-CS, 3D plot). (a) Traditional method, showing only the false tracks. (b) New method, showing the false tracks and disguising the true target.

by the jammer). After converting these tracks to the common ECF coordinate system, the radar fusion center will display six tracks, with each radar system contributing three tracks.

All the tracks in the fusion center are shown in Fig. 11. To investigate the performance, we also compare the new cooperative deception method with the traditional range-only deception method. Define ''traditional method'' as that showing only range deception tracks, and define ''new method'' as that not only showing false tracks but also disguising the true target.

Fig. 11(a) is the result of the traditional method (the jammer generates only a range false target with fixed delay $\Delta R = 3$km both for radar A and B), and Fig. 11(b) is our newly presented method, not only showing false tracks but also disguising the true target (the parameters are $\{\rho_1 = 2, \rho_2 = 0.5\}$). From Fig. 11(a), it can be seen that the target tracks gather together and that the jammer tracks also gather together, being perturbed only by the EKF noise. The reason for this outcome is simple: the target and the jammer are both physical targets, and they have unique global space positions at some points, irrespective of the radar viewing angle. However, from Fig. 11(b), we know that if the new method is implemented, then at every time, there will be a range deception decoy (with time-varying delay) that can form a noncoherent dual-source angle deception effect with the true target to be protected. As a result, the angle measurement of the true target for each radar system is actually biased. In fact, in Fig. 11(b), the track-to-track association distance of the target is obviously larger than that of the jammer itself. This phenomenon can also be viewed more clearly in the 2D projection plane, as shown in Fig. 12, where the diffusion and aggregation effects are more obvious. It must be pointed out that in the initial steps, there exist some perturbations wherein the EKF needs time to converge to a stable state.

Next, we investigate the average track-to-track distance with different measurement errors and different methods. To compare the performances, we consider two radar measurement accuracies: higher measurement accuracy ($\sigma_R = 10$m, $\sigma_A = \sigma_E = 1$mard) and lower measurement accuracy ($\sigma_R = 100$m, $\sigma_A = \sigma_E = 10$mard).

Tables 1–4 show the average track-to-track association distances with respect to the traditional method and the presented new method, where Table 1 and Table 2 have higher measurement accuracy and Table 3 and Table 4 have lower measurement accuracy. The track-to-track association is compared with all possible cases such that we can obtain six association pairs. The track-to-track association distance is computed according to (51) and averaged among all time instants, producing a total of approximately 371 samples.

The higher measurement error cases are shown in Table 1 and Table 2. From Table 1, it can be seen that the mean track-to-track association distances of the physical targets (i.e., the target and the jammer itself) are very small, with values of only $d = 126.41$m and $d = 117.71$m, which accounts for the filtering errors. Actually, assume that the EKF estimation error is nearly consistent; then, the theoretical threshold is $\Delta d \approx 3(p_{11}^{\mathrm{A}} + p_{22}^{\mathrm{A}} + p_{33}^{\mathrm{A}} + p_{11}^{\mathrm{B}} + p_{22}^{\mathrm{B}} + p_{33}^{\mathrm{B}})^{1/2}$, where $p_{ii}^{\mathrm{X}} (i = 1, 2, 3; \mathrm{X} = \mathrm{A,B})$ is the element of the covariance $\mathbf{P}_{k|k}^{\mathrm{X}}$ in the ECF-CS. In the above simulation, the average threshold is approximately $\Delta d = 311.94$m; thus, they both satisfy the discrimination rule $d \leq \Delta d$ and can be judged as two physical targets. For the classical range deception method, although the decoys can form stable and high-fidelity tracks in an individual radar indicator, they cannot deceive the fusion center, as can be seen in Table 1. All the decoy-related track-to-track associations both have larger association distances and will be ruled out by the fusion-center-based ''common origin'' test principle. However, this dilemma has been overcome by the newly presented method. As can be seen in Table 2, after using dual-source jamming, the target signal can have relatively large biased angle measurements, and consequently, when these tracks are sent to the fusion center, the track-to-track association distance of the two radar systems is very large and might

TABLE 1. Average track-to-track association distances (in meters): traditional method with higher measurement accuracy.

	Target (Radar B)	Jammer (Radar B)	Decoy ΔR=3 km (Radar B)
Target (Radar A)	126.41	6289.75	8734.68
Jammer (Radar A)	6340.59	117.71	3033.04
Decoy ΔR=3 km (Radar A)	8276.13	3101.30	2930.37

TABLE 2. Average track-to-track association distances (in meters): New method with higher measurement accuracy.

	Target (Radar B)	Jammer (Radar B)	Decoy ΔR=3 km (Radar B)
Target (Radar A)	1777.32	5292.74	7811.71
Jammer (Radar A)	5488.51	128.12	3052.14
Decoy ΔR=3 km (Radar A)	7600.82	3158.36	2894.94

TABLE 3. Average track-to-track association distances (in meters): traditional method with lower measurement accuracy.

	Target (Radar B)	Jammer (Radar B)	Decoy ΔR=3 km (Radar B)
Target (Radar A)	1088.12	6288.05	9023.15
Jammer (Radar A)	7249.98	1564.88	3589.88
Decoy ΔR=3 km (Radar A)	8656.33	3478.32	3465.27

not pass the "common origin" test. Actually, in Table 2, the track-to-track association distance of the target is as large as $d = 1777.32\text{m} > \Delta\text{d} = 311.94\text{m}$ and can be judged as originating from non-common sources. This indicates that using the cooperative deception jamming method will greatly increase the track-to-track association distance and reduce the discrimination ability of the fusion center.

The lower measurement error cases are shown in Table 3 and Table 4. It can be seen that when the measurement error is larger, for physical targets, the track-to-track association distance will increase rapidly; however, this is not the case for decoys with the same deception parameters. In Table 3, the track-to-track association distance of the target itself (observed by the two radar systems) is 1088.12 m, which accounts for the average filtering noise level. However, in Table 4, we can observe that the new method has an average track-to-track association distance of 1927.66 m for the true target to be protected. Since 1927.66 m is only slightly larger than 1088.12 m, we can conclude that in this case, the jamming effect might not be satisfactory; thus, the true target will not be disguised and might be judged as a physical target. Thus, we can draw the following conclusion: the smaller the given radar measurement error is, the higher the rejection probability of the true target obtained.

TABLE 4. Average track-to-track association distances (in meters): New method with lower measurement accuracy.

	Target (Radar B)	Jammer (Radar B)	Decoy ΔR=3 km (Radar B)
Target (Radar A)	1927.66	5374.98	8081.33
Jammer (Radar A)	6380.85	1445.25	3528.26
Decoy ΔR=3 km (Radar A)	7915.34	3421.78	3567.21

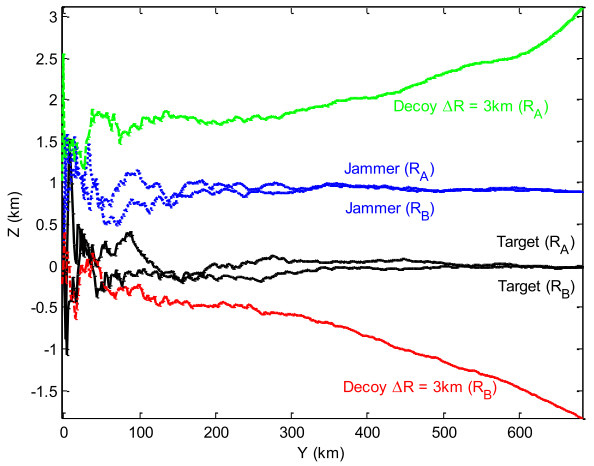

(a) Traditional method.

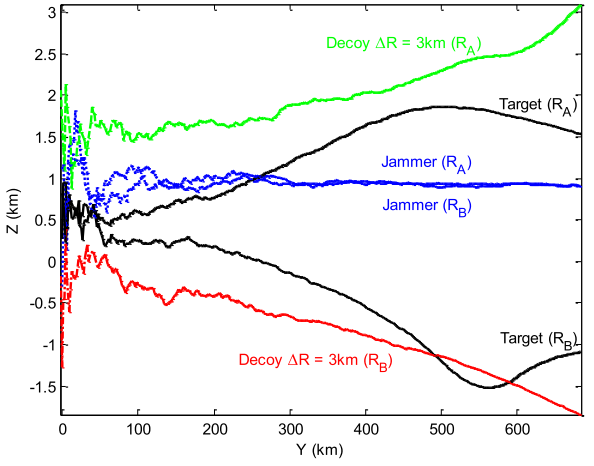

(b) New method.

FIGURE 12. All tracks in the fusion center (ECF-CS, Z-Y plane plot). (a) Traditional method, showing only the false tracks. (b) New method, showing the false tracks and disguising the true target.

F. "NON-COMMON ORIGIN" TEST PROBABILITIES

Next, we investigate the rejection probabilities of the true target in detail. The judgment is made according to 10000 Monte Carlo simulations to compute the rejection ("non-common") probabilities of the true target under different retransmitted amplitude ratios.

From Fig. 12, some conclusions are obvious; we briefly summarize them in the following:

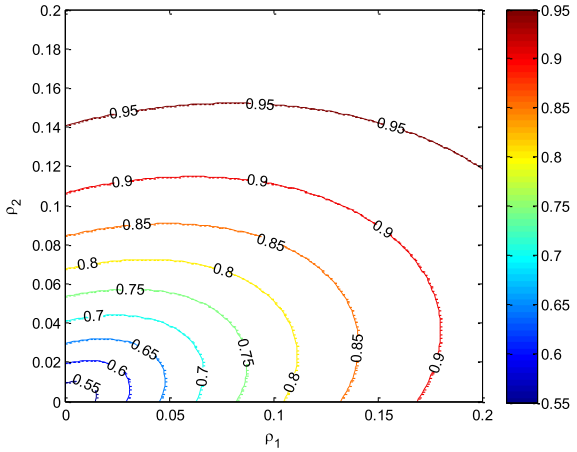

(a) Higher measurement accuracy

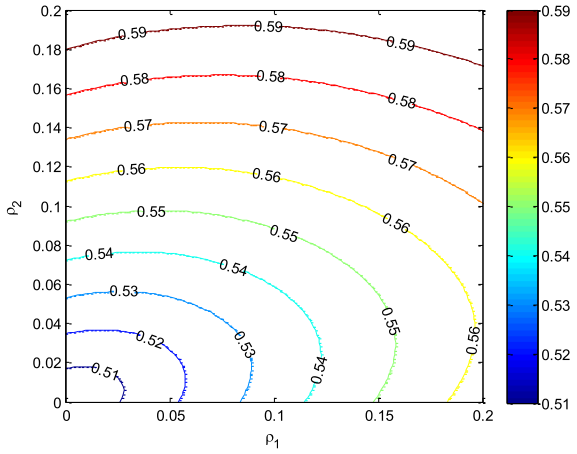

(b) Lower measurement accuracy

FIGURE 13. **" Non-common origin" probabilities of the true target. (a) Higher measurement accuracy, with $\sigma_R = 10$m and $\sigma_A = \sigma_E = 1$mard. (b) Lower measurement accuracy, with $\sigma_R = 100$m and $\sigma_A = \sigma_E = 10$mard.**

(i) The larger the values of the relative amplitude ratios ρ_1 and ρ_2 are, the higher the rejection probability of the true target obtained.

(ii) The smaller the given radar measurement error is, the higher the rejection probability of the true target obtained.

From Fig. 13, it can be seen that the only condition under which the true target will pass the "common origin" test is $(\rho_1 = 0, \rho_2 = 0)$, which accounts for the special case of no jamming. Apart from this, in a general case, ρ_1 and ρ_2 with arbitrary nonzero values will have a jamming effect, even in the special case $(\rho_1 = 1, \rho_2 = 1)$. Actually, when $(\rho_1 = 1, \rho_2 = 1)$, the rejection probability of the true target is still 1; we do not show their values in Fig. 13 for the sake of conciseness and brevity. In fact, $(\rho_1 = 1, \rho_2 = 1)$ means that only the measurements of the true target might be intensively perturbed, but it does not mean that the track-to-track distance is as small as zero. Thus, for a general case, our presented method is valid. Regarding Fig. 13(a), if the amplitude ratio satisfies $(\rho_1 > 0.2, \rho_2 > 0.14)$, then we can guarantee that the rejection probabilities of the true target are larger than 95%.

V. CONCLUSION

One of the major challenges for jamming networked radar systems arises from the native "common origin" signature of physical targets, wherein defense radar systems using a simple track-to-track association can easily rule out most of the jamming tracks.

To defeat distributed radar fusion, this paper proposes a cooperative method where jamming signals and the true target signal can form the noncoherent dual-source angle deception effect by controlling the delay and amplitude. The emphasis is on cooperation between the true target and the jammer such that a decoy can appear in the same range ring as that of the true target as well as in the same beam. The results indicate that by applying the new cooperative angle deception, it can destroy the "common origin" signature of the true target of interest. Thus, true targets might not be discriminated by the fusion center; thereby, the effect of "disguise true target and show false target" can be partly realized.

This approach can be easily extended to multiple-jammer and multiple-target scenarios. Actually, a single jammer can counter only radar systems in the same frequency band, and in general, the trajectory of the jammer itself cannot be modified. Perhaps multiple jammers combined with multiple targets can realize a much better jamming effect; this consideration requires further investigation.

ACKNOWLEDGMENT

The authors appreciate the careful and valuable comments of the editors and anonymous reviewers, on the basis of which the quality of this paper was improved.

REFERENCES

[1] S. Blackman and R. Popoli, *Design and Analysis of Modern Tracking Systems*. Boston, MA, USA: Artech House, 1999.

[2] Y. Bar-Shalom, and W. D. Blair, *Multitarget-Multisensor Tracking: Applications and Advances*, vol. 3. Norwood, MA, USA: Artech House, 2000.

[3] Y. Bar-Shalom, and X. R. Li, *Multitarget-Multisensor Tracking: Principles and Techniques*. Storrs, CT, USA: YBS Publishing, 1995.

[4] Y. Bar-Shalom, P. K. Willett, and X. Tian, *Tracking and Data Fusion: A Handbook of Algorithms*. Storrs, CT, USA: YBS Publishing, 2011.

[5] R. P. S. Mahler, *Statistical Multisource-Multitarget Information Fusion*. Norwood, MA, USA: Artech House, 2007.

[6] H. Wang, J. Johnson, C. Baker, L. Ye, and C. Zhang, "On spectrum sharing between communications and air traffic control radar systems," in *Proc. IEEE Radar Conf. (RadarCon)*, Washington, DC, USA, May 2015, pp. 1545–1550.

[7] F. Meyer, O. Hlinka, H. Wymeersch, E. Riegler, and F. Hlawatsch, "Distributed localization and tracking of mobile networks including noncooperative objects," *IEEE Trans. Signal Inf. Process. Netw.*, vol. 2, no. 1, pp. 57–71, Mar. 2016.

[8] J.-H. Lim, D.-W. Lim, B. L. Cheong, and M.-S. Song, "Spectrum sharing in weather radar networked system: Design and experimentation," *IEEE Sensors J.*, vol. 19, no. 5, pp. 1720–1729, Mar. 2019.

[9] X. Wang, L. Xu, H. Sun, J. Xin, and N. Zheng, "On-road vehicle detection and tracking using MMW radar and monovision fusion," *IEEE Trans. Intell. Transp. Syst.*, vol. 17, no. 7, pp. 2075–2084, Jul. 2016.

[10] M. Nouri, M. Mivehchy, and M. F. Sabahi, "Novel anti-deception jamming method by measuring phase noise of oscillators in LFMCW tracking radar sensor networks," *IEEE Access*, vol. 5, pp. 11455–11467, 2017.

[11] L. Lan, G. Liao, J. Xu, Y. Zhang, and F. Fioranelli, "Suppression approach to main-beam deceptive jamming in FDA-MIMO radar using nonhomogeneous sample detection," *IEEE Access*, vol. 6, pp. 34582–34597, 2018.

[12] F. A. Butt, I. H. Naqvi, and A. I. Najam, "Radar ECCM against deception jamming: A novel approach using bi-static and mono-static radars," in *Proc. 15th Int. Multitopic Conf. (INMIC)*, Islamabad, Pakistan, Dec. 2012, pp. 137–141.
[13] S. Zhao, L. Zhang, Y. Zhou, and N. Liu, "Signal fusion-based algorithms to discriminate between radar targets and deception jamming in distributed multiple-radar architectures," *IEEE Sensors J.*, vol. 15, no. 11, pp. 6697–6706, Nov. 2015.
[14] S. Zhao, N. Liu, L. Zhang, Y. Zhou, and Q. Li, "Discrimination of deception targets in multistatic radar based on clustering analysis," *IEEE Sensors J.*, vol. 16, no. 8, pp. 2500–2508, Apr. 2017.
[15] C. Yang, L. Feng, H. Zhang, S. He, and Z. Shi, "A novel data fusion algorithm to combat false data injection attacks in networked radar systems," *IEEE Trans. Signal Inf. Process. Netw.*, vol. 4, no. 1, pp. 125–136, Mar. 2018.
[16] H. Chen and T. Kirubarajan, "Performance limits of track-to-track fusion versus centralized estimation: Theory and application," *IEEE Trans. Aerosp. Electron. Syst.*, vol. 39, no. 2, pp. 386–400, Apr. 2003.
[17] X. Gao, J. Chen, D. Tao, and X. Li, "Multi-sensor centralized fusion without measurement noise covariance by variational Bayesian approximation," *IEEE Trans. Aerosp. Electron. Syst.*, vol. 47, no. 1, pp. 272–718, Jan. 2011.
[18] X. Feng, Y.-N. Zhao, Z.-F. Zhao, and Z.-Q. Zhou, "Cognitive tracking waveform design based on multiple model interaction and measurement information fusion," *IEEE Access*, vol. 6, pp. 30680–30690, 2018.
[19] M. E. Liggins, C.-Y. Chong, I. Kadar, M. G. Alford, V. Vannicola, and S. Thomopoulos, "Distributed fusion architectures and algorithms for target tracking," *Proc. IEEE*, vol. 85, no. 1, pp. 95–107, Jan. 1997.
[20] Y. Bar-Shalom, "On the track-to-track correlation problem," *IEEE Trans. Autom. Control*, vol. AC-26, no. 2, pp. 571–572, Apr. 1981.
[21] K. C. Chang, R. Saha, and Y. Bar-Shalom, "On optimal track fusion," *IEEE Trans. Aerosp. Electron. Syst.*, vol. 33, no. 4, pp. 1271–1276, Oct. 1997.
[22] Y. Bar-Shalom and H. Chen, "Multisensor track-to-track association for tracks with dependent errors," *J. Adv. Inf. Fusion*, vol. 1, no. 1, pp. 3–14, 2006.
[23] Y. Bar-Shalom and H. Chen, "Track-to-track association using attributes," *J. Adv. Inf. Fusion*, vol. 2, no. 1, pp. 49–59, Jun. 2007.
[24] W. Mei and G.-L. Shan, "Performance of a multiscan track-to-track association technique," *Signal Process.*, vol. 85, no. 1, pp. 15–22, Jan. 2005.
[25] D. E. Maurer, "Information handover for track-to-track correlation," *Inf. Fusion*, vol. 4, no. 4, pp. 281–295, Dec. 2003.
[26] N. J. Willis, *Bistatic Radar*. Boston, MA, USA: Artech House, 1991.
[27] P. F. Howland, "Target tracking using television-based bistatic radar," *IEE Proc.-Radar, Sonar Navigat.*, vol. 146, no. 3, pp. 166–174, Jul. 1999.
[28] T. Sathyan, A. Sinha, and T. Kirubarajan, "Passive geolocation and tracking of an unknown number of emitters," *IEEE Trans. Aerosp. Electron. Syst.*, vol. 42, no. 2, pp. 740–750, Apr. 2006.
[29] K. R. Pattipati, S. Deb, Y. Bar-Shalom, and R. B. Washburn, "A new relaxation algorithm and passive sensor data association," *IEEE Trans. Autom. Control*, vol. 37, no. 2, pp. 198–213, Feb. 1992.
[30] M. I. Skolnik, *Radar Handbook*, 3rd ed. New York, NY, USA: McGraw-Hill, 2008.
[31] D. C. Schleher, *Electronic Warfare in the Information Age*. Boston, MA, USA: Artech House, 2000.
[32] S. D. Berger, "Digital radio frequency memory linear range gate stealer spectrum," *IEEE Trans. Aerosp. Electron. Syst.*, vol. 39, no. 2, pp. 725–735, Apr. 2003.
[33] P. A. Ingwersen and W. Z. Lemnios, "Radars for ballistic missile defense research," *Lincoln Lab. J.*, vol. 12, no. 2, pp. 245–266, Feb. 2000.
[34] J. E. Lindsay, "Angular glint and the moving, rotating, complex radar target," *IEEE Trans. Aerosp. Electron. Syst.*, vol. AES-4, no. 2, pp. 164–173, Mar. 1968.
[35] H. Yin and P. Huang, "Unification and comparison between two concepts of radar target angular glint," *IEEE Trans. Aerosp. Electron. Syst.*, vol. 31, no. 2, pp. 778–783, Apr. 1995.
[36] X. R. Li, B. J. Slocumb, and P. D. West, "Tracking in the presence of range deception ECM and clutter by decomposition and fusion," in *Proc. Signal Data Process. Small Targets*, Denver, CO, USA, Oct. 1999, pp. 198–210.
[37] X. R. Li and V. P. Jilkov, "Survey of maneuvering target tracking—Part II: Motion models of ballistic and space targets," *IEEE Trans. Aerosp. Electron. Syst.*, vol. 46, no. 1, pp. 96–119, Jan. 2010.
[38] T. H. Kerr, "Streamlining measurement iteration for EKF target tracking," *IEEE Trans. Aerosp. Electron. Syst.*, vol. 27, no. 2, pp. 408–421, Mar. 1991.
[39] G. M. Siouris, G. Chen, and J. Wang, "Tracking an incoming ballistic missile using an extended interval Kalman filter," *IEEE Trans. Aerosp. Electron. Syst.*, vol. 33, no. 1, pp. 232–240, Jan. 1997.
[40] G. P. Cardillo, A. V. Mrstik, and T. Plambeck, "A track filter for reentry objects with uncertain drag," *IEEE Trans. Aerosp. Electron. Syst.*, vol. 35, no. 2, pp. 394–409, Apr. 1999.
[41] A. Farina, B. Ristic, and D. Benvenuti, "Tracking a ballistic target: Comparison of several nonlinear filters," *IEEE Trans. Aerosp. Electron. Syst.*, vol. 38, no. 3, pp. 854–867, Jul. 2002.
[42] B. Rao, S. Xiao, and X. Wang, "Joint tracking and discrimination of exoatmospheric active decoys using nine-dimensional parameter-augmented EKF," *Signal Process.*, vol. 91, no. 10, pp. 2247–2258, Oct. 2011.
[43] B. Rao, Y.-L. Zhao, S.-P. Xiao, and X.-S. Wang, "Discrimination of exo-atmospheric active decoys using acceleration information," *IET Radar, Sonar Navigat.*, vol. 4, no. 4, pp. 626–638, Apr. 2010.
[44] B. Rao, S. Xiao, X. Wang, and T. Wang, "Maximum likelihood approach to the estimation and discrimination of exoatmospheric active phantom tracks using motion features," *IEEE Trans. Aerosp. Electron. Syst.*, vol. 48, no. 1, pp. 794–819, Jan. 2012.